# THE PARTICLE-IN-CELL CODE BENDER AND ITS APPLICATION TO NON-RELATIVISTIC BEAM TRANSPORT

D. Noll*, M. Droba, O. Meusel, U. Ratzinger, K. Schulte, C. Wiesner
Institute of Applied Physics, Goethe University Frankfurt am Main

*Abstract*

A new non-relativistic, electrostatic Particle-in-Cell code named bender has been implemented to facilitate the investigation of low-energy beam transport scenarios. In the case of high-intensity beams, space-charge compensation resulting from the accumulation of secondary particles – electrons for positively charged ion beams – is an important effect. It has been shown, that the distribution of compensation electrons can have a significant influence on the beam and lead to an emittance growth. To improve the understanding of the dynamics of the compensation and the resultant self-consistent steady state, ionization of residual gas as well as secondary electron production on surfaces have been implemented and used to study a number of test systems. We will present first results of these compensation studies as well as further applications of the code, among them the chopper section of the future FRANZ facility [1].

## IMPLEMENTATION

The Particle-in-Cell [2] code bender is written in the C++ language and uses MPI for parallelisation. It reads input files in an XML-style format. All numerical values in this file are affixed with units. The output of the code can be configured to include particle distributions and losses, field and potential distribution and single particle tracks, as required.

External fields can either be loaded from data exported from tools like the CST Suite or Opera, calculated numerically via either the solution of Laplace's equation on a lattice or from the Biot-Savart law by integrating the current flow through wires defined by analytic expressions, or calculated from several available field models, including multipole field distributions and several solenoid field models.

For use as boundaries for either particle movement or the Poisson solver, various geometric primitives like planes, tubes and plates are implemented. For more complex geometries, an import from STL files is available.

All geometric objects in the code can then be transformed by one or multiple affine transformations, which allows objects like fields, geometric objects, monitors and even poisson solvers to be placed in the simulation "space" at will.

To simulate dc beams, a fixed number of particles, spread out over $v_{\mathrm{beam}}\Delta t$, are inserted in every time step, continuously building up the beam volume.

### *Field Solvers*

The code provides three solvers for Poisson's equation.

For problems requiring either non-equidistant grid spacing or geometrically complex boundary conditions, there is a cartesian solver using a Shortley-Weller finite-difference stencil [3]

$$\frac{\varphi_{i-1,j,k}}{\Delta_-\,(\Delta_+ + \Delta_-)} - \frac{\varphi_{i,j,k}}{\Delta_+\Delta_-} + \frac{\varphi_{i+1,j,k}}{\Delta_+\,(\Delta_+ + \Delta_-)} + \text{other dir.} = -\frac{\rho_{i,j,k}}{2\epsilon_0} + O(\Delta^3), \qquad (1)$$

where $\Delta_\pm$ are the distances to either the neighbouring grid points or a grid boundary. Dirichlet, Neumann and periodic boundary conditions on the grid boundaries can be considered. The grid can be distributed among processors in blocks in all directions, which allows bent geometries to be followed without wasting memory on inactive regions. An example is shown in Fig. 1.

On initialisation of the solver, all processors calculate the positions and the sizes of boundary surfaces with their neighbours. In a second step, intersections between the grid lines and the boundary objects given for the solver are calculated in multiple passes over each direction. In the first of the three passes, grid points not contained in any boundary object are assigned a global index. When an intersection with an object is found on the line between two grid points, its position is stored for the respective active grid point using its index. In a third step, the geometric information gathered is communicated in the bounding areas found in the first step.

After mesh generation, a sparse matrix for the potential on the grid points is constructed using Eq. (1). To solve this matrix, the PetSc library [4] is used. After the solution process, to be able to calculate the electric field in the region between the grid portions local to two processors, potential

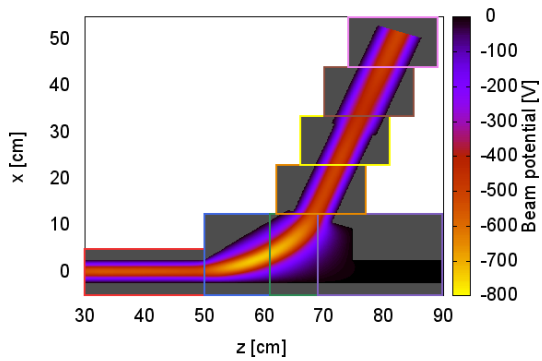


Figure 1: Example of a calculation of electric potential of a guided electron beam on 16 processors. The coloured rectangles show the grid portions on each processor. Each domain is additionally split in vertical direction. The grey portions of the grid are disabled on each processor, the white portions are not considered by any processor.

* noll@iap.uni-frankfurt.de



ISBN 978-3-95450-173-1

values from the neighbouring processors are required and are therefore communicated.

For simulations of radially symmetric systems, the code includes an rz finite difference solver also using the PETSc library. In the case only a rectangular grid with equidistant spacing is required, a 3d xyz solver using Fourier's method implemented using the FFTW library [5] can be used. Both of these solvers allow for Dirichlet, Neumann or periodic boundary conditions and can be distributed among processors in longitudinal direction.

All three solvers don't require particles to be local to their grid portions. However, when requested, particles can be distributed among processors according to each processors portion of the grid, reducing the amount of communication in the field accumulation step.

### *Particle Pusher*

Bender implements various algorithms for integration of particle motion, among others one using the standard RK4 integration algorithm and a symplectic Euler integrator. The (non-relativistic) algorithm used in the simulations presented below is

$$r_{i+1} = r_i + \frac{\Delta t}{m}\left(p_i + \Delta p_i\right)$$
$$p_{i+1} = p_i + A_{i+1}^{-1}\left(p_i + \Delta p_i + \frac{q\Delta t}{2}E_{i+1}\right)$$
$$\Delta p_{i+1} = \frac{q\Delta t}{2}E_{i+1} + \lambda p_{i+1} \times B_{i+1},$$

where $r_i$ and $p_i$ are the particles position and momentum in the $i$'th step, $q$ and $m$ its charge and mass, $\Delta p$ was defined to avoid recalculation between adjacent time steps, $\lambda = q\Delta t/\left(2m\right)$ and

$$A_i = \begin{pmatrix} 1 & -\lambda B_i^z & \lambda B_i^y \\ \lambda B_i^z & 1 & -\lambda B_i^x \\ -\lambda B_i^y & \lambda B_i^x & 1 \end{pmatrix}.$$

The implementation was compared to several analytically solvable test cases and showed second order accuracy as well as long time energy conservation.

## SPACE CHARGE COMPENSATION

Two processes lead to the production of electrons in positive low-energy ion beams: impact ionisation of residual gas atoms and molecules and secondary particle production due to the impact of particles on the beam pipe. These electrons can then be trapped inside the beams positive potential, reducing it until a steady-state is produced.

The amount of electrons produced per meter per second by a beam of energy $E$, current $I$ in a homogeneous residual gas background of pressure $p$ and temperature $T$ is given by

$$\nu = \frac{Ip\sigma(E)}{ekT},$$

where $\sigma(E)$ is the total proton impact ionisation cross section. For $I = 100\,\mathrm{mA}$, $E = 120\,\mathrm{keV}$ protons on $p = 1\times10^{-3}$ Pa, T=300 K $N_2$, $\nu = 8\times10^{15}$ electrons/s/m are produced. The energy of most of these electrons is not large enough for them to cause additional ionisation. However, in high-intensity beams, the space charge potential can be high enough for electrons to gain sufficient energy to ionise additional gas molecules.

Secondary electron production on surfaces for protons is in the order of a few electrons per impact, depending on energy, impact angle and surface composition. Thus, if significant portions of the beam (0.6 % for the parameters given above) are lost, this mechanism dominates residual gas ionisation. However, since these electrons are created at zero potential, it is unclear if they are able to remain in the system for long times.

For the simulation, Argon was considered as a residual gas, as a compromise between absolute value – lower cross section meaning longer simulation time –, complexity of the residual gas ions – for $H_2$ for example, $H_2^+$ and $H^+ + H^0$ are produced–, and data availability.

Ionising collisions were implemented in bender using the Null-collision method [6]. Argon is considered as an homogeneously distributed ideal gas. Single-differential cross section data for proton impact ionisation were taken from [7]. Electron impact cross section data is calculated from the Binary-Encounter-Bethe-model [8]. The velocities of the freed electrons are then distributed isotropically. Under the assumption, that the remaining, very low-energy ion travels in the direction of the projectile, the deflection angle of the projectile and the energy of the residual gas ion can be calculated from energy and momentum conservation.

### *Compensation Without Magnetic Fields*

Initially a system without any magnetic focussing elements was investigated. A 100 mA, 120 keV beam with an emittance of 100 mm mrad was matched through a 50 cm drift section in a way, that avoids particle losses at 0 % to 100 % compensation. The section is bounded by two repeller

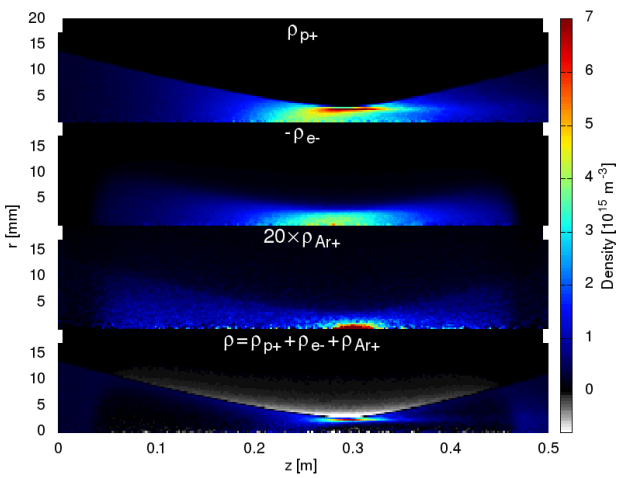


Figure 2: Proton, electron, residual gas ion and total charge densities for the simulation of a 50 cm long drift system.

ISBN 978-3-95450-173-1

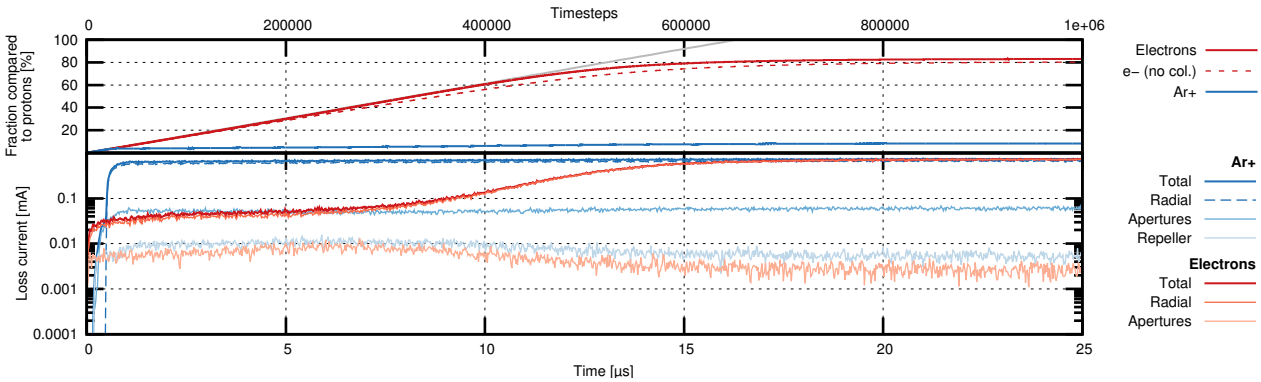


Figure 3: Global compensation degree and particle losses from the compensation simulation of a 50 cm drift. The compensation degree is plotted for two simulations – one including electron impact ionisation and one with just proton impact ionisation ("no col."). Particle losses are registered on the repeller electrodes at the end of the system and on the beam tube in radial direction. Some ions as well as a small amount of electrons created inside the repeller are accelerated out of the simulation volume longitudinally through the repeller apertures.

electrodes at −1.5 kV potential to trap electrons longitudinally.

Simulation runs were made using either the rz- oder the fast fourier poisson solver, on a grid of either $\Delta r = 0.1$ mm, $\Delta z = 0.2$ mm or $\Delta x = \Delta y = 0.4$ mm, $\Delta z = 1.7$ mm. The time step used was $\Delta t = 25$ ps. On 12 processors of the "Fuchs" cluster [9] using the rz solver and 50 macroparticles inserted per step, simulation time is about 1 day for 25 µs.

Figure 3 shows the global compensation degree during built-up of compensation. For the first 10 µs, the compensation degree follows

$$\eta_{\mathrm{comp}}(t) = \frac{\nu_{\mathrm{beam}} e}{I} \nu t,$$

which means, that only a negligible amount of electrons is able to escape the confinement.

After the initial linear increase, at about 7 ns, the potential is sufficiently reduced for electrons to start escaping. After 17 ns the electron loss current – almost exclusively in radial direction – equals the current of residual gas ions. At this point, an equilibrium is reached, with a global compensation degree of 80.7 %. The introduction of electron impact ionisation increases this value to 83.3 %.

The argon ions produced by ionisation are constantly accelerated out of the system radially. The amount of ions in the system slowly increases during the built-up, due to the decrease in space charge potential. In the steady-state, argon ions are responsible for an additional positive charge of 8 % of the beams charge.

The densities in the steady-state of the system are shown in Fig. 2.

It was found, that the electron velocities at a given longitudinal position follow a Gaussian profile. This would suggest that the system is in a thermodynamic equilibrium. The temperature is neither isotropic, $T_x \approx T_y \neq T_z$, nor is it equal everywhere in the system. Table 1 shows the plasma parameters for the electrons at the position of the beams focus.

Table 1: Plasma Parameters of Compensation Electrons at $z = 28$ cm

| | | | | | |
|---|---|---|---|---|---|
| $T_x$ | 34.1 | eV | $\lambda_d$ | 0.7 | mm |
| $T_y$ | 33.7 | eV | $\omega_p$ | 0.5 | GHz |
| $T_z$ | 48.1 | eV | $\ln\Lambda$ | 16.6 | |
| $n_e$ | $3.9 \times 10^{15}$ | $\mathrm{m}^{-3}$ | | | |

For such a system, a self-consistent solution of the Poisson-Boltzmann equation given in 1d under the assumption of a radially symmetric and longitudinally homogeneous system

$$\frac{1}{r}\frac{\mathrm{d}}{\mathrm{d}r}\left(r\frac{\mathrm{d}\varphi(r)}{\mathrm{d}r}\right) = -\frac{1}{\epsilon_0}\left(\rho_{\mathrm{beam}}(r) - \rho_e(r)\right),$$
$$\rho_{\mathrm{e}}(r) = \rho_0 \exp\left\{-\frac{e\varphi(r)}{kT}\right\} \qquad (2)$$

should provide the spatial distribution of the compensation electrons. $\rho_0$ can be determined by setting the total electron charge to a fraction $\eta_{\mathrm{comp}}$ of the beams total charge,

$$\int_0^R \mathrm{d}r\, r\rho_{\mathrm{beam}}(r) = \rho_0\eta_{\mathrm{comp}} \int_0^R \mathrm{d}r\, r\rho_{\mathrm{e}}(r). \qquad (3)$$

Figure 4 shows the solution of Eq. (2) and (3) in comparison to the bender solution. Except for an excess of electrons close to the axis – probably a result from the presence of the residual gas ions – the simulation agrees very well to the simple 1d theory. In general, this means that for finite electron temperatures even at 100% space charge compensation, there is some remaining space charge force on the beam.

The source of the thermal distribution is yet unclear, and could be a result of (numerical) noise in the particle distributions. In a physical system with the parameters given in Tab. 1, particles should relax to a thermal distribution due to Coulomb collisions on a timescale of [10]

$$\tau_{ee} = 3\pi(2\pi)^{1/2}\frac{\epsilon_0^2(kT)^{3/2}}{n_e e^4 m^{1/2}\ln\Lambda} \approx 0.5\,\mathrm{ms}.$$



ISBN 978-3-95450-173-1

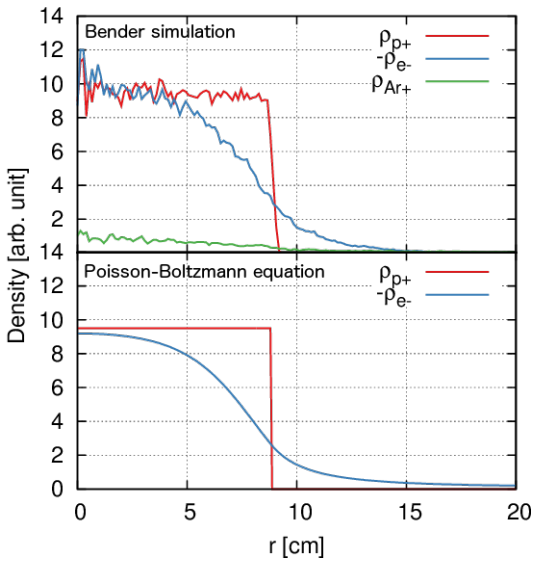


Figure 4: Radial electron distribution at $z = 10$ cm from the solution of the Poisson-Boltzmann equation (2) in comparison to the bender simulation for the drift system using the fast fourier solver. $\eta = 90.6\,\%$ and $T = 22.9$ eV.

In the simulation however, a thermal electron distribution can be observed as early as a µs. So far, we have found no significant dependance of the resulting temperatures on simulation parameters, except for the choice of solver geometry. Comparing simulations done using the Fourier solver to the 2d rz-case, the latter shows an excess of electrons with low absolute velocities.

### *Simulation of a Two-solenoid LEBT*

As a next step, simulation runs for a two-solenoid beam transport section using the rz solver were made. The 1.6 m long section includes two 25 cm long solenoids at 0.7 T to match the beam without any losses.

In these simulations, no steady-state was reached. Especially in the fringe field regions of the solenoid near the axis, low-energy electrons and residual gas ions accumulate, leading to a linear increase in the number of particles for these species. This spurious accumulation of residual gas ions near the axis was also found in the 2d simulations made for the drift section, where it does not grow indefinitely however. It is noticeably absent in the simulations made using the 3d fast fourier solver. Several ways to ameliorate the situation such as incorporating the dynamics of the background gas (either dynamically or by including a fixed profile) or including recombination have been suggested.

As for the case of the simple drift, a double layer forms at the edge of the beam in between the two solenoids. In the center of the solenoids however, electrons are strongly bound to the field lines. Thus the size of the double layer is greatly reduced there.

## SIMULATION OF THE FRANZ E×B CHOPPER

The E×B chopper concept, designed for high-repetition chopping of a 50 mA, 120 keV proton beam at the Frankfurt Neutron Source FRANZ [11], uses magnetostatic deflection to safely dump the unwanted beam fraction, which is compensated for short periods of time by a voltage pulse to two deflection plates to provide short beam pulses in forward direction. The copper was successfully commissioned using a low-energy helium beam [1]. The layout is shown in Fig. 5.

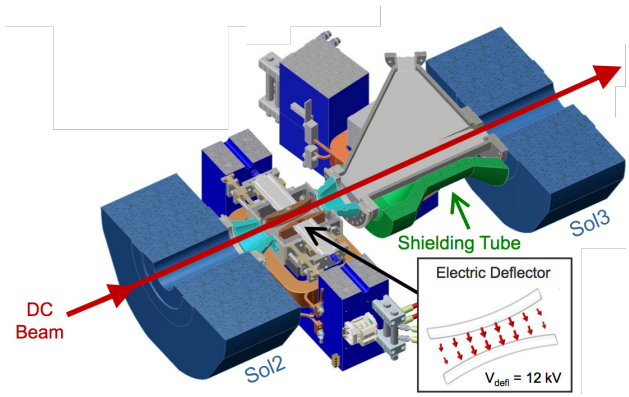


Figure 5: Layout of the E×B chopper located between solenoid 2 and 3 of the FRANZ low-energy beam transport section.

Magnetic and electric fields were simulated using the CST Suite and imported into bender. There is some magnetic flux from and to the H-type dipole magnet, which provides static beam deflection, into the adjacent solenoid magnets, which are used to match the beam to the chopper and the chopped beam to the following RFQ. To capture this effect in the simulation and still be able to independently adjust field levels, each magnet was simulated in the whole setup but with every other magnet turned of.

First, single particle tracking using bender was used to understand the distortions produced by the crossed electric and magnetic field configuration [12]. After optimisation of the field geometry, simulations including space charge of the 50 mA proton beam were made. In addition to the proton beam, the simulation includes 5 mA of $H_2^+$ and 5 mA of $H_3^+$ ions produced by the ion source. The input distribution at the start of the section were taken from 2D matching simulations of the LEBT. The voltage pulse on the deflection plates was taken from measurements of the pulse generator.

The geometry of the chopper system was included in the solution of the electric field of the proton beam. Simulations were made using a mesh of 2.5 mm in each direction distributed on 10-20 processors of the CSC cluster "Fuchs" [9].

Figure 6 shows the particle distribution at a time step during the fall time of the voltage pulse. The beam is swept over an aperture of 20 mm radius. Both the $H_2^+$ and the $H_3^+$ ions are deflected too strongly, so that only particles in the flanks of the pulse are transmitted into the following section.

ISBN 978-3-95450-173-1

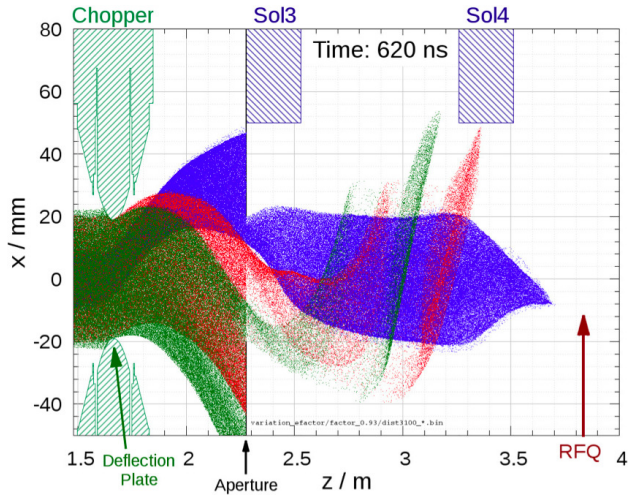


Figure 6: Snapshot of the chopper simulation, 50 mA proton beam (blue), 5 mA $H_2^+$ (red) and 5 mA (green).

Transmission of the proton beam through the aperture is, by design, 100%.

Simulations show, that the design flat-top pulse length of 50 ns can be reached with low beam offset below ±0.3 mm. The total pulse length is 350 ns. A large fraction of the pulse flanks has considerable position offset and will be collimated at the RFQ entrance. However, it was found, that the long pulse length compared to the flat top helps to mediate the effect of longitudinal broadening of the pulse by space charge forces compared to (theoretical) pulses of more step-wise distribution.

## CONCLUSION AND OUTLOOK

The dynamics of space charge compensation has been studied for some geometrically simple systems using a Particle-in-Cell code developed at IAP. For a system without any magnetic field, a thermal distribution of compensation electrons has been found. Furthermore, the code has been used extensively for the investigation of the E×B chopper concept including space charge.

Additionally, bender is in use for several other projects, including simulation of beam injection into a figure-8 storage ring [13], beam dynamics in CH cavities, simulation of electron beams in an electron lens for the IOTA ring at Fermilab [14] and simulation of plasma dynamics in Gabor lenses [15].

## REFERENCES

[1] C. Wiesner et al., Experimental Performance of an E×B Chopper System, Proc. of IPAC 2014, THPME015 (2014).

[2] C. K. Hockney, A. B. Langdon, Plasma Physics via Computer Simulation, CRC Press (2004).

[3] G. H. Shortley, R. Weller, The Numerical Solution of Laplace's Equation, J. Appl. Phys. 9, 334 (1938).

[4] S. Balay, S. Abhyankar, M. F. Adams, J. Brown, P. Brune, K. Buschelman, V. Eijkhout, W. D. Gropp, D. Kaushik, M. G. Knepley, L. C. McInnes, K. Rupp, B. F. Smith, H. Zhang, PETSc Web page, http://www.mcs.anl.gov/petsc

[5] M. Frigo, S. G. Johnson, The Design and Implementation of FFTW3, Proceedings of the IEEE 2005, 93, 2, Special issue on "Program Generation, Optimization, and Platform Adaptation"(2005).

[6] V. Vahedi, M. Surendra, A Monte Carlo collision model for the particle-in-cell method: applications to argon and oxygen discharges, Computer Physics Communications 87, 1-2, p. 179-198, 1995.

[7] M. E. Rudd, Y.-K. Kim, D. H. Madison and T. J. Gay, Electron production in proton collisions with atoms and molecules: energy distributions, Reviews of Modern Physics 64, 2, p. 441 (1992).

[8] Y.-K. Kim and M. E. Rudd, Binary-encounter-dipole model for electron-impact ionization, Phys. Rev. A 50, 5, p. 3954 (1994).

[9] Center for Scientific Computing Cluster "Fuchs", http://hhlr.csc.uni-frankfurt.de/

[10] R. J. Goldston, P. H. Rutherford, Introduction to Plasma Physics, Institute of Physics Pub. (1995).

[11] C. Wiesner et al., Proton Driver Linac for the Frankfurt Neutron Source, AIP Conf. Proc. 1265, 487 (2010).

[12] C. Wiesner et al., Chopping High Intensity Proton Beams Using a Pulsed Wien Filter, Proc. of IPAC 2012 (2012).

[13] Droba, M., Ates, A., Meusel, O., Niebuhr, H., Noll, D., Ratzinger, U., Wagner, J., Simulation Studies on Beam Injection Into a Figure-8 Type Storage Ring, Proc. of IPAC2014, TUPRO045(2014).

[14] G. Stancari, Applications of electron lenses: scraping of high-power beams, beam-beam compensation, and nonlinear optics, arXiv 1409.3615 (2014).

[15] K. Schulte et al., Space-Charge Compensation of Intense Ion-Beams by Nonneutral Plasma Columns, Proc. of HB2014, MOPAB19 (2014).



ISBN 978-3-95450-173-1